Dalton Transactions

Accepted Manuscript

ROYAL SOCIETY OF CHEMISTRY

www.rsc.org/dalton

Journal Name

ARTICLE

Structural characterization of magnesium silicate hydrate: towards the design of eco-sustainable cements

Received 00th January 20xx,
Accepted 00th January 20xx

DOI: 10.1039/x0xx00000x

www.rsc.org/

M. Tonelli[a]‡, F. Martini[b]‡, L. Calucci[b], E. Fratini[a], M. Geppi[c], F. Ridi[a]*, S. Borsacchi[b]* and P. Baglioni[a]

Magnesium based cement represents one of the most interesting eco-sustainable alternatives to standard cementitious binders. The interest towards this material has a twofold reason: *i*) its production process, taking place from magnesium silicates, brine or seawater, dramatically reduces the CO_2 emissions with respect to those connected with the Portland cement production and *ii*) it is very well suited to applications for radioactive waste encapsulation. In spite of its potential, the assessment of the structural properties of its binder phase (magnesium silicate hydrate or M-S-H) is far from complete, especially because of its amorphous character. In this work, a comprehensive structural characterization of M-S-H was obtained by means of a multi-technique approach, including a detailed Solid State NMR investigation and, in particular, for the first time, quantitative ^{29}Si Solid State NMR data. M-S-H was prepared through room temperature hydration of highly reactive MgO and silica fume and was monitored for 28 days. The results clearly evidenced the presence in M-S-H of "chrysotile-like" and "talc-like" sub-nanometric domains, which are approximately in a 1:1 molar ratio for long time hydration. Both these kinds of domains have a high degree of condensation, corresponding to the presence of a small amount of silanols in the tetrahedral sheets. The decisive improvement obtained in the knowledge of the M-S-H structure paves the way for tailoring the macroscopic properties of eco-sustainable cements by means of a bottom-up approach.

1. Introduction

In the last decade, research efforts on the investigation of magnesium-based cements have significantly grown for two main reasons both concerning sustainable chemistry: they can be employed for radioactive waste encapsulation,[1–3] and, most important, have been recognized as promising alternative to the common CaO-based (Portland) cements in applications requiring pH lower than 11.[4-6] The great amount of emitted CO_2 associated with the manufacturing of Portland cement, in fact, claims for urgent measures to move towards eco-sustainable strategies in the field of building materials production.[7–11] Magnesium-based cements are generally obtained by hydration of reactive periclase (MgO) in the presence of silica sources, to produce magnesium silicate hydrate (M-S-H) gel. [12–17] Because of the low abundance of natural MgO, some sustainable processes to obtain reactive MgO starting from abundant sources have been recently proposed. One viable solution is to obtain reactive periclase from magnesium silicates (among the main constituents of the Earth crust) according to the method developed by a start-up company of the Imperial College of London.[18] Another possibility, which is gaining a renewed interest in the scientific community, is the production of reactive MgO from the treatment of brine or seawater.[19] Obtaining MgO from these alternative sources largely reduces CO_2 emissions with respect to those associated with the production of Portland cement. The use of magnesium-based cements in real applications at the moment is restricted, mainly because of the limited comprehension of both the structure of the M-S-H gel and the hydration process that causes its precipitation. Furthermore, the mechanical properties of MgO-based cements are inferior to those of traditional cements[5] limiting their use to specific applications. The literature on Portland cement and, in particular, on the structural properties of C-S-H clearly demonstrated that a deep understanding of the microstructure is essential in order to predict the macro-scale mechanical properties.[20] For this reason, the planning of a serious scale-up of the production of any new building material requires an in depth multi-scale investigation of the structural properties. So far, the reported studies on MgO-based cements have evidenced that the properties of M-S-H depend on temperature,[17] on the relative amounts of reagents,[21] and on the reactivity of precursors. [12,22,23] Recent

a) Department of Chemistry "Ugo Schiff" & CSGI, University of Florence, Sesto Fiorentino 50019, Florence, Italy. E-mail: francesca.ridi@unifi.it ; Telephone: +39-055-4573015.
b) Istituto di Chimica dei Composti OrganoMetallici, Consiglio Nazionale delle Ricerche – CNR U.O.S. di Pisa, Pisa 56124, Italy. E-mail: silvia.borsacchi@pi.iccom.cnr.it ; Telephone +39-050-3153052.
c) Department of Chemistry and Industrial Chemistry, University of Pisa, Pisa 56124, Italy.
The manuscript was written through contributions of all authors. All authors have given approval to the final version of the manuscript.
‡These authors contributed equally.
Electronic Supplementary Information (ESI) available: pH measurements, mass losses from TG measurements, ^{1}H-^{29}Si CP-MAS spectra, FTIR spectra deconvolution. See DOI: 10.1039/x0xx00000x

papers have been reported on the characterization of the reaction products[3,14] and on the investigation of the M-S-H microstructure by using small angle scattering techniques,[24] but a full characterization of this binder is still lacking.

In this study, the hydration product at ambient conditions of a mixture of highly reactive MgO and silica fume has been characterized during the first 28 days. No plasticizing polymers have been added, in order to investigate the structure of the pristine M-S-H gel, and reactants have been chosen to favour the formation of the hydrated phase. We adopted a multi-technique approach (Solid State NMR, Infrared Spectroscopy, X-Ray Powder Diffraction, Scanning Electron Microscopy, Differential Thermal Analysis, Thermogravimetry) aiming at the complete characterization of the material. Solid State NMR (SSNMR) is an extremely powerful technique for the investigation of the structural properties of complex solid materials, either crystalline or amorphous.[25] In particular, ^{29}Si SSNMR has been extensively applied to the study of traditional CaO-based cements, largely contributing to the definition of the structural model of the amorphous C-S-H binding phase.[26] On the contrary, the application of SSNMR to M-S-H has been relatively limited so far; in particular only ^{29}Si and, in some cases, ^{25}Mg monodimensional spectra, giving qualitative information on M-S-H gels obtained by means of different strategies, have been reported.[3,21,27–31] In this work we applied for the first time quantitative ^{29}Si measurements, combined with ^{1}H and two-dimensional ^{1}H-^{29}Si experiments, to the products of hydration of the MgO/SiO_2 mixture, with the aim of gaining insights into the structural features of the M-S-H binding phase on a molecular and sub-nanometric scale.

2. Experimental Section

2.1. Materials

Periclase (MgO) and silica fume were supplied by Sigma-Aldrich. The main characteristics of these powders are summarized in Table 1. The reactivity of periclase was measured according to the test proposed by van der Merwe et al.[32] and resulted to be 80 s, which indicates that the powder is highly reactive.

Table 1. Characteristics of the reagents.

Reagent	Particle average size (by gas sorption analysis)	Purity	Specific surface [m^2/g]
MgO	44 μm	> 99 %	121 ± 5
SiO_2	5 μm*	> 99 %	395 ± 25

* this size results from the agglomeration of 7 nm particles (as declared by Sigma)

MgO and SiO_2 were mixed in a 1:1 molar ratio. The MgO/SiO_2 (MS) paste was prepared by manually mixing typically 4 g of solids with 8 g of milliQ water, i.e. at a water-to-solid weight ratio (w/s) of 2. The paste was stored at 20 °C in a polyethylene bag to avoid air contact and prevent carbonation. After 1, 7 and 28 days from the preparation, roughly 1 g of paste was withdrawn and freeze-dried to stop the hydration reaction. An abbreviated notation has been used throughout the paper to refer to MS paste freeze-dried at different days of hydration: MS_1d (1 day), MS_7d (7 days) and MS_28d (28 days).

2.2. Methods

pH measurements were performed with a BASIC 20 Crison pH-meter using the method previously described by Zhang et al.[5] Briefly, 1 g of the paste was added to a polyethylene container with 10 g of distilled water. The tube was then sealed and constantly stirred in an orbital shaker. At different time intervals, the solid particles were allowed to settle and the pH of the supernatant was measured.

Fourier transform infrared (FTIR) spectra were acquired between 4000 and 400 cm^{-1} by means of a NEXUS 870-FTIR (Thermo Nicolet, Fitchburg, WI, USA) spectrometer with a DTGS TEC detector (32 scans, resolution of 2 cm^{-1}). 1 mg of each sample was homogenized with 100 mg of KBr and pressed to obtain a pellet.

Thermogravimetry (TG) was conducted on a STD Q600 (TA Instruments, Philadelphia, USA) instrument, operating from room temperature to 1000 °C at 10 °C/min, in nitrogen flux.

X-ray (XRD) diffractograms were recorded with a XRD Bruker New D8 Da Vinci instrument operating at 40 kV and 40 mA, with a Cu source (emitting radiation at a wavelength of 1.54 Å). The scanning region was in the 2θ range 5°÷70°, with 0.05°/step. XRD spectra were recorded on MS_1d, MS_7d, MS_28d samples before and after heating at 900 °C.

Scanning Electron Microscopy (SEM) images were collected on uncoated fracture surfaces with a field-emission ΣIGMA (Carl Zeiss) microscope, with an accelerating potential of 2 kV. Surface area measurements were performed by means of a Coulter SA 3100 analyser.

Solid State NMR (SSNMR) experiments were carried out on a Varian InfinityPlus 400 spectrometer working at ^{1}H and ^{29}Si Larmor frequency of 400.35 and 79.48 MHz, respectively, equipped with 3.2 and 7.5 mm probeheads. 1D ^{29}Si experiments were carried out using the 7.5 mm probehead, spinning the samples at a MAS frequency of 5.5 kHz and under ^{1}H high-power decoupling. The ^{29}Si Direct Excitation-Magic Angle Spinning (DE-MAS) spectra were recorded using a 90° excitation pulse with a duration of 6 μs, a recycle delay of 20 s, and accumulating 4000 transients. ^{1}H-^{29}Si Cross Polarization (CP)-MAS spectra at variable contact time were recorded using a linear ramp for CP and a ^{1}H TPPM high-power decoupling, with a recycle delay of 2 s. ^{29}Si T_1's were determined using a saturation-recovery pulse sequence with a train of 100 90° saturating pulses and recovery delays between 0.01 and 600 s, accumulating, for each delay value, 180 transients. ^{1}H MAS and ^{1}H-^{29}Si FSLG-HETCOR experiments were carried out on the 3.2 mm probehead at a MAS frequency of 20 kHz. ^{1}H MAS spectra were recorded accumulating 32 transients with a recycle delay of 2 s, while the ^{1}H-^{29}Si FSLG-HETCOR spectrum was recorded with a contact time of 0.6 ms (which was chosen for having enough magnetization transfer from protons to silicon nuclei, at the same time minimizing the effects of proton spin-

diffusion), accumulating 1968 transients per 64 rows. All the experiments were performed at room temperature, using air as spinning gas. Tetramethyl silane was used as a primary chemical shift reference for all nuclei, while 3-(trimethylsilyl)-1-propane-sulfonic acid sodium salt and isopropanol were employed as secondary references for ^{29}Si and ^{1}H, respectively.

3. Results

3.1. pH measurements

pH measurements (Figure S1, Supporting Information) were performed on hydrated MS proving the advancement of the reaction over a period of 28 days. In the first hours the pH value is affected by the presence of brucite ($Mg(OH)_2$), which is reported to have $pK_a \approx 10.5$. After 3 days, the pH of the sample decreases to ~9 because of the consumption of brucite in the reaction with hydrated silica and, then, it remains stabilized at this value up to 28 days. The observed pH trend is well in agreement with the description recently provided by Li et al.[14] and it indicates that, from 3 to at least 28 days of hydration, the sample maintains the optimal pH value to promote the precipitation of M-S-H gel.[12,14]

3.2. TG/DTA analysis

Figure 1A illustrates the weight losses from room temperature up to 1000 °C registered by means of thermogravimetric analysis on MS paste samples freeze-dried after 1, 7 and 28 days of hydration (MS_1d, MS_7d and MS_28d). Three principal mass losses can be observed (Table S1 of Supporting Information): one from room temperature to about 200 °C, the second approximately in the 310-400 °C range, and the last ending around 800 °C. The first can be attributed to the loss of physisorbed water still present after the freeze-drying process. The second loss is ascribed to the dehydroxylation of residual brucite formed by hydration of MgO and not reacted with silica.[13] The mass loss at higher temperature arises from the decomposition of M-S-H due to the loss of its hydroxyl groups.[13]

Figure 1B shows the DTA data for the MS_1d, MS_7d and MS_28d samples. The endothermic events around 100 °C and 400 °C correspond to the mass loss from M-S-H and $Mg(OH)_2$, respectively. An exothermic event, which is not associated to a mass loss, is registered for all the investigated samples between 800 and 900 °C. According to the literature, this effect is due to a solid phase transition of M-S-H to crystalline species.[3,13] This thermal feature progressively sharpens during the hydration, also shifting at lower temperatures. Similar crystallization events have been reported for the thermal treatment of amorphous talc, which is converted to enstatite ($MgSiO_3$)[33] and for the thermal treatment of chrysotile, which brings to a mixture of enstatite and forsterite (Mg_2SiO_4).[34] In the thermograms of MS_1d and MS_7d two exothermic peaks are observed at ~850 °C, indicating the formation of two crystalline species. To further understand the transformations associated with these exothermic effects, structural XRD analyses and ^{29}Si SSNMR experiments have been performed on samples heated to 900 °C , which are reported in Sections 3.3 and 3.4, respectively.

For a detailed investigation of the decomposition of the different phases present in the samples, we calculated the first derivative of the thermogravimetric curves and we performed a deconvolution of the obtained DTG curves with Gaussian functions.[35-37] Figure 2 illustrates the results of the analysis and Table 2 reports the parameters (temperature of the maximum, T_{max}, and area) of each Gaussian peak.

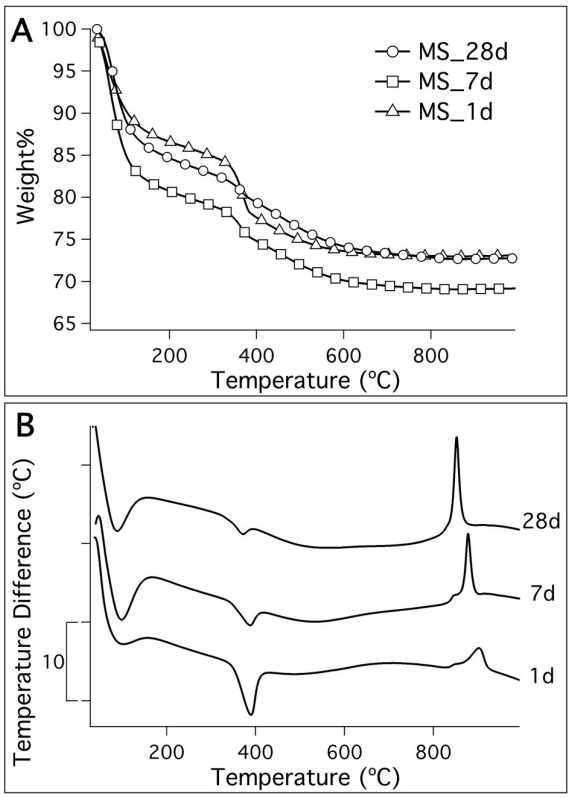

Figure 1. A) TG scans of MS_1d, MS_7d and MS_28d. B) DTA profiles of MS_1d, MS_7d and MS_28d. The DTA curves have been offset for the sake of clarity.

Two peaks (#1 and #2) are present from room temperature to 200 °C. The area of #1 increases in the first week of hydration and then slightly decreases. Peak #2 appears at lower temperature for the MS_1d sample with respect to samples MS_7d and MS_28d and has a markedly larger area: this is probably due to a significant contribution from water adsorbed on reagents (especially SiO_2) not yet reacted after 1 day. According to the literature,[3] #1 can be assigned to water adsorbed on M-S-H surface, which increases until the binder phase formation is almost completed, while #2, once the reagents have reacted completely, is due to water confined in the pores of M-S-H.[13] T_{max} of these peaks shifts to higher temperature with hydration time, probably because M-S-H pores decrease in size with the advancement of the reaction, causing a strengthening in the water/M-S-H interactions and, therefore, an increase in the evaporation temperature. A shift to higher temperature is also observed for the large peak in the 200-800 °C range (#4), which is assigned to the dehydroxylation of M-S-H.[13] The sharp peak at about 360 °C

(#3) is due to $Mg(OH)_2$ dehydroxylation: its area decreases as a function of the hydration time, because brucite is converted to M-S-H.

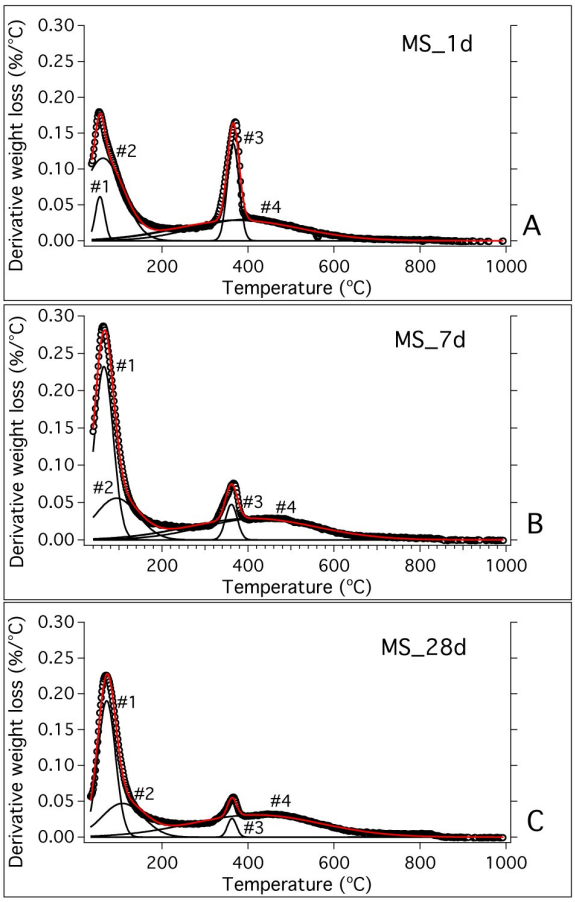

Figure 2. Deconvolution of the DTG curves of (A) MS_1d, (B) MS_7d and (C) MS_28d samples. Black markers represent the experimental data, red lines are the global fitting curves; the single Gaussian peaks obtained by the fitting procedure are shown as black lines.

Table 2. Position and percentage area of the Gaussian peaks resulting from the deconvolution of DTG curves. Uncertainties are reported in parentheses.

		MS_1d	MS_7d	MS_28d
Peak 1	T_{max} /°C (±5)	55	65	71
	Area/ % (±8%)	6	40	35
Peak 2	T_{max} /°C (±5)	62	94	109
	Area/ % (±10%)	45	21	21
Peak 3	T_{max} /°C (±3)	365	361	363
	Area/ % (±1%)	15	3	3
Peak 4	T_{max} /°C (±5)	376	409	418
	Area/ % (±15%)	34	34	41

3.3. XRD analysis

Figure 3 (top) shows the XRD diffractograms of MS_1d, MS_7d and MS_28d. In all cases brucite appears as the main crystalline phase. In the MS_1d diffractogram only a small peak due to periclase is present, indicating that after 24 hours almost all the MgO is hydrated. This peak completely disappears after 7 days. According to previous studies,[12,21] the broad peaks typical of an amorphous phase, observed in the 5-10°, 17-28°, 32-39° and 58-62° ranges, are consistent with the XRD pattern of the M-S-H phase. By following the evolution of the XRD diffractograms during the hydration, it is observed that the intensity of the brucite peaks decreases as time passes, while that of the M-S-H signals increases.

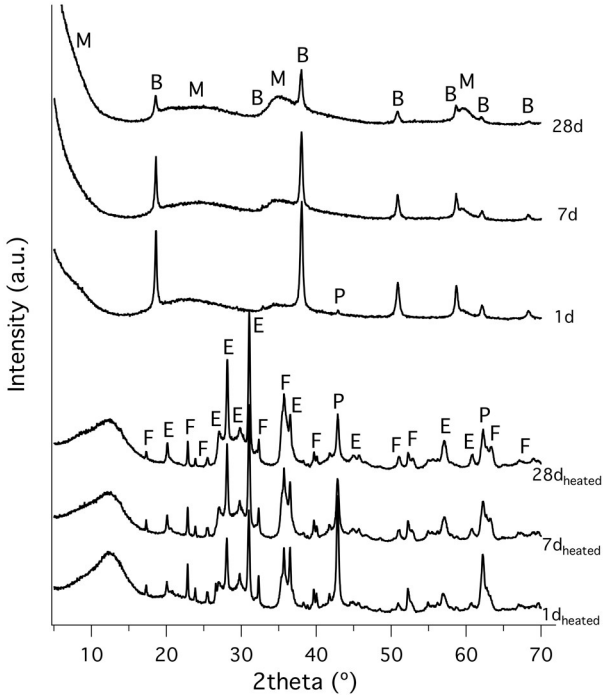

Figure 3. XRD patterns of MS_1d, MS_7d and MS_28d samples before and after heating to 900 °C. Curves have been offset for the sake of clarity. M: M-S-H; B: brucite; P: periclase; E: enstatite; F: forsterite.

In order to better characterize the phases formed at high temperature, as indicated by DTA, XRD diffractograms were also recorded on MS_1d, MS_7d and MS_28d samples after heating to 900 °C. A similar analysis was recently reported by Walling et al.[3] XRD patterns of heated samples (bottom part of Figure 3) revealed the presence of periclase [AMCSD: 0000501], forsterite [AMCSD: 0000276], and clinoenstatite [AMCSD: 0010589] crystalline phases. Periclase derives from the dehydroxylation of brucite upon heating, while forsterite and clinoenstatite are anhydrous magnesium silicates arising from M-S-H. Clinoenstatite is a polymorph of enstatite, already observed as a crystallization product of heated M-S-H gels, here recognized from the characteristic ^{29}Si SSNMR signals (vide infra).

3.4 Solid State NMR investigation

3.4.1. ^{29}Si spectra

^{29}Si DE-MAS spectra of MS pastes freeze-dried after 1, 7 and 28 days of hydration are reported in Figure 4. All the spectra show quite broad and partially overlapped signals, as expected considering the amorphous character of both silica and M-S-H. Typical signals of M-S-H[3,21,27–31] and silica can be recognized in the spectral regions approximately between -100 and -75 ppm,

and between -125 and -95 ppm, respectively. In order to identify the different signals, the spectra were fitted using the minimum number of peaks necessary for an accurate reproduction. The analysis of the spectrum of MS_28d allowed five M-S-H signals to be identified. In particular two peaks were found at -79.6 and -82.1 ppm, which can be ascribed to different Q^1 $\underline{Si}(OMg)(OSi)(OH)_2$ species, indicated as Q^{1A} and Q^{1B}, respectively. One signal was identified at -86.3 ppm due to Q^2 $\underline{Si}(OMg)(OSi)_2OH$ sites. Two peaks, centred at -92.9 and -95.2 ppm and ascribed to two different Q^3 $\underline{Si}(OMg)(OSi)_3$ silicon sites (Q^{3A} and Q^{3B}), were necessary for obtaining an accurate reproduction of the intense signal at the lowest chemical shift. The presence of two peaks underlying the Q^3 signal is also evident from the asymmetry of its lineshape in the ^1H-^{29}Si CP-MAS spectra recorded at different contact times (Figure S2 of the Supporting Information), one of which is shown in Figure 4. Moreover, the trends of the peak areas vs contact time, obtained for the Q^1, Q^2 and Q^3 peaks provided interesting information. In the fast CP regime ($T_{SiH} < T_{1\rho}^H$), which has been found to be valid for all the silicon nuclei of M-S-H (see Supporting Information), the increasing trend of the signal intensity at short contact times is governed by the so called cross-polarization time constant, T_{SiH}. Considering that T_{SiH} usually increases decreasing the number of ^1H nuclei spatially close to ^{29}Si nuclei, the trend T_{SiH} (Q^{1A})≈ T_{SiH} (Q^{1B})≈ T_{SiH} (Q^2) < T_{SiH} (Q^{3A}) < T_{SiH} (Q^{3B}) obtained for the MS_28d sample corroborates the signal assignment and suggests that Q^{3A} silicons have a larger number of close protons (Mg-OH) than Q^{3B} silicons.

The ^{29}Si DE-MAS spectra of MS_7d and MS_1d samples could be well reproduced using the same peaks that fitted the spectrum of MS_28d (keeping fixed the chemical shifts, linewidths and Lorentzian/Gaussian ratios to the values reported in Table 3, and varying the intensities), with the addition of two peaks for the Q^4 ($\underline{Si}(OSi)_4$) and Q^3 ($\underline{Si}(OSi)_3OH$) sites of silica at -111.5 and -102.0 ppm, respectively (Table 3). It must be said that in the case of MS_1d, due to the presence of an intense Q^3 silica signal, a comparably good spectral reproduction was obtained also with a sole M-S-H Q^3 peak centred at -93.5 ppm. Moreover an additional peak was found at -78.5 ppm for MS_1d and MS_7d, but, also considered the corresponding T_1 value, as it will be better discussed in Section 3.4.4, we believe that it arises from some anhydrous magnesium silicate species, as for example $MgSiO_3$.[27] In the spectra of MS_7d and MS_28d a very weak but reproducible signal can be observed at -63 ppm, which could be tentatively assigned to another anhydrous form of magnesium silicate: for example a chemical shift of -62 ppm has been reported for forsterite.[27,34]

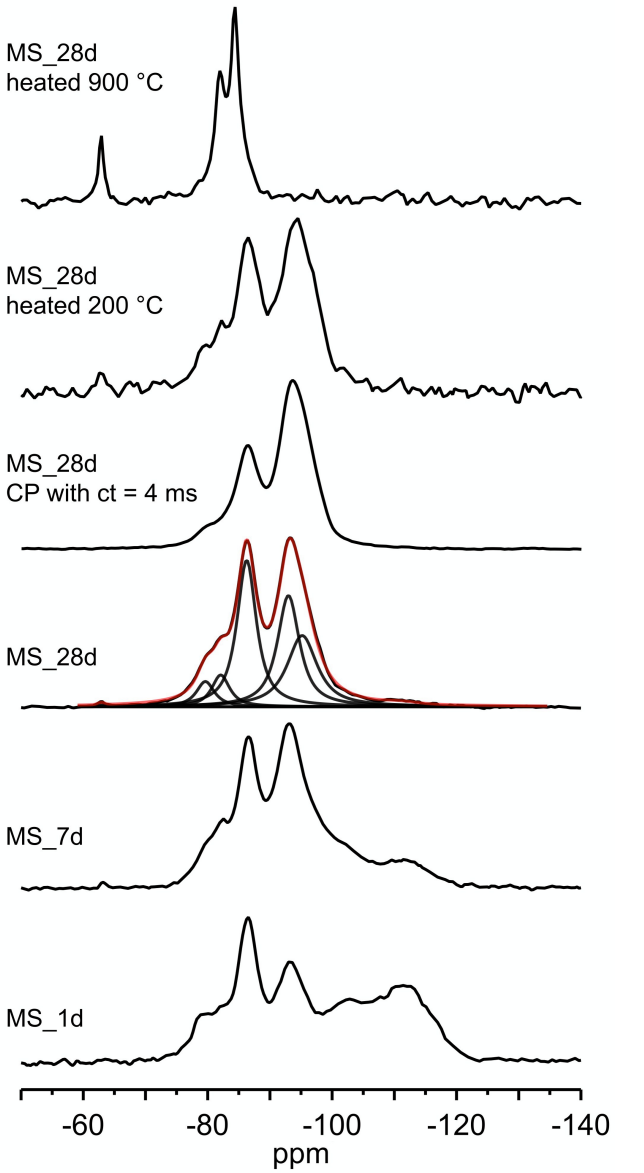

Figure 4. ^{29}Si DE-MAS spectra of MS_1d, MS_7d and MS_28d samples and of MS_28d heated to 200 °C and to 900 °C. For MS_28d the fitted DE-MAS spectrum, with the single peaks (in black), is reported (in red) over the experimental spectrum. The ^1H-^{29}Si CP-MAS spectrum of MS_28d, recorded with a contact time of 4 ms, is also shown.

In order to obtain quantitative information from ^{29}Si spectra, the areas obtained from the fittings were suitably scaled on the basis of the corresponding ^{29}Si T_1 values, as it will be described in Section 3.4.4. The quantitative areas so obtained, which are directly proportional to the amount of the corresponding silicon nuclei, are reported in Table 3. The results clearly show that about 40% of silica is consumed in the first 24 hours; after 7 days its amount is further halved and after 28 days an almost negligible amount remains. The faster decrease of the Q^4 signal with respect to Q^3 is in agreement with the fact that the reaction of silica with MgO is preceded

Journal Name

ARTICLE

Table 3. Results obtained from the analysis of ^{29}Si SSNMR data. In the first lines the chemical shift (δ) and linewidth (Δ) of the peaks obtained by fitting the ^{29}Si DE-MAS spectra of MS_1d, MS_7d, MS_28d are reported. A Lorentzian to Gaussian ratio (L/G) of 0.9 and 0.2 was used for M-S-H and silica peaks, respectively. In the second block of lines quantitative values of the areas underlying the peaks are reported as A%. As described in the text, A% values were obtained by multiplying the areas obtained from the fitting of the ^{29}Si DE-MAS spectra by the respective scaling factors, also reported in the table. The scaling factors were determined from ^{29}Si T_1's measured for MS_28d. Values of T_1 and of the exponent β of the stretched exponential function used for fitting ^{29}Si magnetization recovery curves are also reported.

	Q^{1A}	Q^{1B}	Q^2	Q^{3A}	Q^{3B}	Q^3 SiO_2	Q^4 SiO_2
δ /ppm	-79.6	-82.1	-86.3	-92.9	-95.2	-102.0	-111.5
Δ / Hz	276	273	297	337	458	570	815
A% MS_1d	2±1	2±1	15±1	10±2	8±1	20±5	44±12
A% MS_7d	2±1	4±1	19±1	22±5	22±2	15±4	17±5
A% MS_28d	4±1	5±1	29±2	29±6	33±2	-	1±1
T_1/s	40±11	59±16	65±7	128±62	99±8	134±38	
β	0.69±0.11	0.62±0.07	0.60±0.03	0.47±0.05	0.75±0.03	1	
Scaling factor	2.2±0.3	2.5±0.4	2.6±0.1	2.9±0.6	3.8±0.2	7±2	7±2

by hydration, which transforms Q^4 into Q^3 sites. In parallel with silica consumption, M-S-H signals increase. Interestingly, within the experimental errors, the ratio Q^2:Q^{3A}:Q^{3B} remains approximately 1:1:1 after 7 days of hydration.

^{29}Si DE-MAS spectra were also recorded for two samples of MS_28d heated, respectively, to 200 and 900 °C (Figure 4). While the former substantially shows the same signals observed for unheated MS_28d, confirming that at this temperature only adsorbed water is removed, the latter has a completely different spectrum, characterized by the coexistence of a signal at -62 ppm, ascribable to forsterite, and two signals at -81 and -84 ppm, previously observed for clinoenstatite,[27,34] in agreement with XRD and DTA results.

3.4.2. ^{1}H spectra

Figure 5 shows ^{1}H-MAS spectra of MS_1d, MS_7d and MS_28d. It is worth to remind that in complex solid materials it is very difficult to completely remove ^{1}H-^{1}H homonuclear dipolar couplings, which are responsible for the scarce spectral resolution observed and for the non-quantitative signal intensities. Nonetheless, in the spectra of MS samples three main signals can be resolved at about 0.8, 4.7, and 6.5 ppm. The first one seems to be structured in three components: the one at 0.4 ppm can be ascribed to MgOH protons of M-S-H with a likely contribution from protons of brucite at similar or lower chemical shift,[38] while the peaks appearing at about 0.8 and 1.3 ppm, observable also in the spectrum of silica (Figure 5), can be due to silanols not involved in hydrogen bonds. The relatively narrow and intense peak resonating at 4.7 ppm can be assigned to physisorbed water present in the sample even after freeze-drying. At last, the broad peak centred at about 6.5 ppm can be ascribed to protons of silanol groups involved in hydrogen bonds, either among themselves or with water, which can itself contribute to this signal. It can be noticed that this signal and that of physisorbed water are also present, even if at slightly different chemical shift, in the spectrum of silica.[39,40]

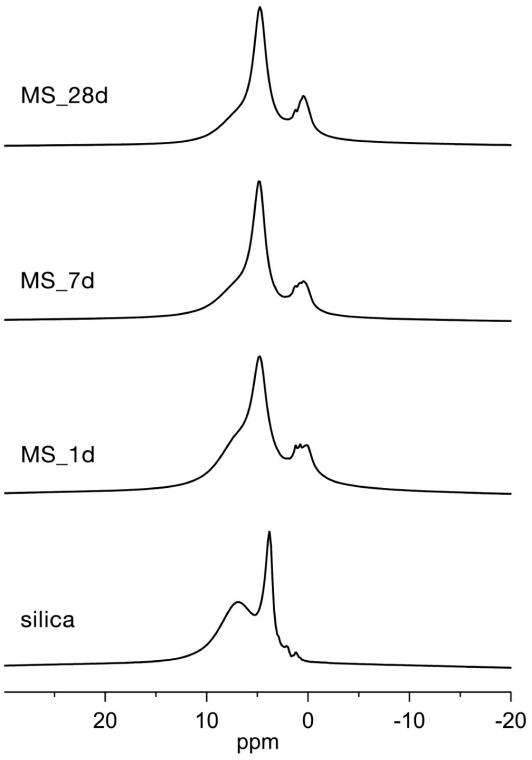

Figure 5. ^{1}H MAS spectra of MS_1d, MS_7d and MS_28d and silica fume samples.

3.4.3. ^{1}H-^{29}Si HETCOR

With the aim of investigating the spatial proximities (of the order of few Å) between silicon and hydrogen nuclei in M-S-H and confirm the ^{29}Si and ^{1}H signal assignment, we recorded a 2D ^{1}H-^{29}Si HETCOR spectrum of MS_28d. In the 2D map, reported in Figure 6, a very intense cross-peak is observed between Q^3 Si(OMg)$(OSi)_3$ silicon and Mg-OH hydrogen nuclei. Correlations are also detected between Q^2 Si(OMg)$(OSi)_2$OH and MgOH (even if a contribution from isolated SiOH cannot be ruled out), as well as hydrogen bonded SiOH protons. Q^1 signals are probably too weak to be detected. The observed correlations confirm the proposed assignment of ^{29}Si and ^{1}H signals to M-S-H. Moreover the absence of correlation with protons of hydrogen-bonded silanols indicates that a possible contribution from Q^2 or Q^1 sites of silica to the peaks ascribed to Q^3 silicon nuclei of M-S-H is negligible.

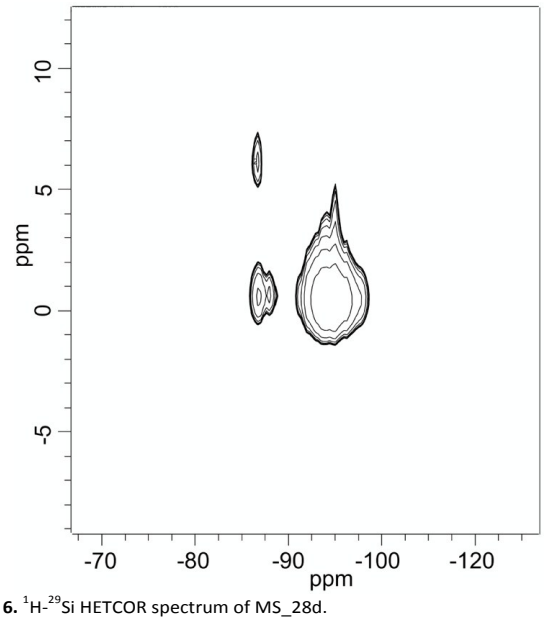

Figure 6. ^{1}H-^{29}Si HETCOR spectrum of MS_28d.

3.4.4. T_1(^{29}Si) and quantitativity of ^{29}Si spectra

As anticipated in Section 3.4.1, the ^{29}Si DE-MAS spectra shown in Figure 4, recorded with a recycle delay between two consecutive transients of 20 s, cannot be *a priori* considered as quantitative, due to the usually very long (tens to hundreds of seconds) ^{29}Si spin-lattice relaxation times T_1's. Indeed, it is known that for obtaining quantitative NMR spectra of an X nucleus, using a direct excitation 90° pulse, a recycle delay at least five times the T_1 of X must be used, which allows the X longitudinal magnetization to fully recover between two consecutive scans. However, the use of a sufficiently long recycle delay would enormously increase the time necessary for obtaining a spectrum with a good signal to noise ratio. Nevertheless it is possible to obtain quantitative information also from spectra acquired with a short recycle delay by using suitable scaling factors which can be determined from T_1 values. To the best of our knowledge, so far ^{29}Si T_1's of M-S-H have not been reported in the literature and the quantitativity of the spectra is only rarely checked or discussed.[27] For this reason we decided to measure ^{29}Si T_1's of M-S-H in MS_28d with a saturation-recovery experiment and use them to obtain quantitative information from our ^{29}Si DE-MAS spectra.[41] For most silicon species the experimental magnetization recovery curves could not be satisfactorily reproduced with a mono-exponential function. On the other hand the curves were well fitted by a stretched exponential function

$$M(t) = M_0(1-\exp(-(t/T_1)^{\beta})$$

with M_0 the equilibrium magnetization and β (0<β≤1) an exponent which takes into account the distribution of different situations intrinsic in the disorder of the system, as pointed out in the literature for diamagnetic amorphous siliceous materials.[42,43] The T_1 and β values obtained are reported in Table 3. An estimate of ^{29}Si T_1 of silica was also obtained by fitting the sum of the areas of its Q^4 and Q^3 signals. Looking at M-S-H signals, it can be observed that T_1 values approximately increase from Q^{1A} and Q^{1B}, to Q^2, to Q^3, in agreement with the decreasing number of bonded OH groups. Indeed the dipolar interaction with spatially close ^{1}H nuclei should decrease the T_1 of ^{29}Si. The silicon species resonating at -78.5 ppm show a particularly long T_1 (150 ± 43 s, with β = 1), suggesting that they could either bear particularly mobile OH groups, or have no OH groups directly bonded.

T_1 values have been used to calculate the scaling factors (*sf*) for the different signals, using the following equation:

$$sf = N/\left(1+N(1-\exp(-(rd/T_1)^{\beta}))\right)$$

where *N* is the number of accumulated transients and *rd* is the recycle delay used.[41] The calculated *sf* values for the different ^{29}Si signals are reported in Table 3, from which it appears evident that spectra recorded with a recycle delay of 20 s cannot be considered as quantitative. Since a large variation of the relaxation times can be reasonably excluded, we used T_1 values measured for MS_28d also for scaling the spectra of MS_1d and MS_7d.

3.5. FTIR spectroscopy

Figure 7 reports the FTIR spectra of the MS samples at different hydration times and of the unhydrated silica and MgO powders, for comparison. Table 4 summarizes the FTIR features present in the spectra. A sharp peak at 3695 cm^{-1}, attributed to brucite,[44] is present in all the spectra of MS samples. The intensity of this peak decreases with hydration time, due to the reaction of brucite with silica. The broad absorption at about 3400 cm^{-1} and the band at 1640 cm^{-1} can be ascribed to OH stretching and bending, respectively. The feature at 1696 cm^{-1} in the silica spectrum may be assigned to Si-OH vibrations,[3] indicating a partial hydration of the powder. In the spectra of silica and MS samples a band composed by multiple absorptions is present in the 1300-850 cm^{-1} range due to the stretching and bending vibrations of Si-O. The peak at about 770 cm^{-1} is attributed to Q^1 Si-O vibrations. The peak at 650 cm^{-1} in the spectrum of MS_28d can be attributed to a

vibration similar to the libration of the Mg_3OH unit in magnesium phyllosilicates.[3] Bands at 560 and 460 cm^{-1} are assigned to MgO vibrations, as can be deduced comparing the spectra of the MS samples with that of MgO.

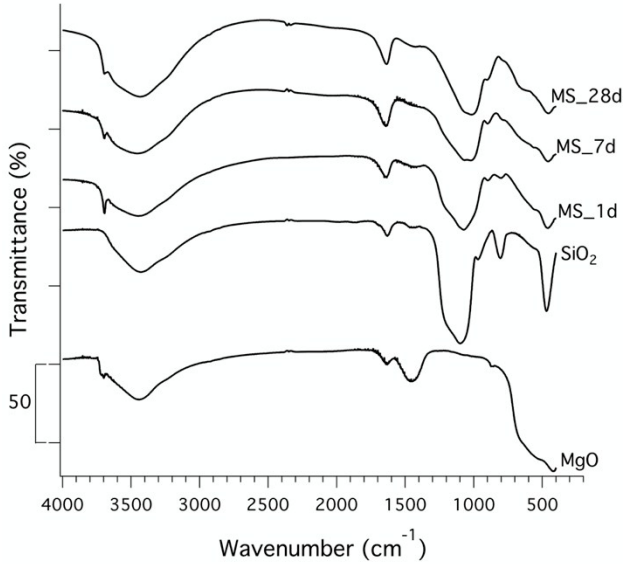

Figure 7. FTIR spectra of MS_1d, MS_7d and MS_28d samples. The spectra of silica and MgO reactants are also reported for comparison. Curves have been offset for the sake of clarity.

Table 4. FTIR data of MS_1d, MS_7d, MS_28d, silica and MgO samples. Key: s-strong; m-medium; w-weak.

	OH vibrations (cm^{-1})	Si-O vibrations (cm^{-1})	Mg-O vibrations (cm^{-1})
MS_1d	3695 m	1213 m	≈1450 m
	3200-3600 m	1078 s	560 w
	1643	987 w	463 s
		884 w	
		805 w	
MS_7d	3695 w	1194 m	≈1450 m
	3200-3600 m	1064 s	565 w
	1642	985 m	461 s
		889 w	
		769 w	
MS_28d	3695 w	1193 m	≈1450 m
	3200-3600 m	1050 s	465 m
	1640	977 w	
	650 w	885 w	
		734 w	
silica	3200-3600 m	1696 w	
	1632 w	1211 s	
		1087 s	
		1030 w	
		951 w	
		808 w	
MgO	3718 w		≈1450 m
	3200-3600 m		560 s
	1637 w		460 s

The deconvolution of the spectra of silica and MS samples in the 1350-850 cm^{-1} spectral range, evidencing the evolution of the silicatic chain polymerization in the growing M-S-H gel, is reported in the Supporting Information as Figure S4 and Table S3.

3.6 SEM analysis

The microscopic analysis performed on MS_28d shows that the M-S-H morphology is rather homogeneous at the microscale level and the globular nature of M-S-H particles becomes evident at high magnification (Fig. 8). The analysis highlighted that these interconnected and densely packed globules have an average size of ~30 nm, in accordance with the literature.[24]

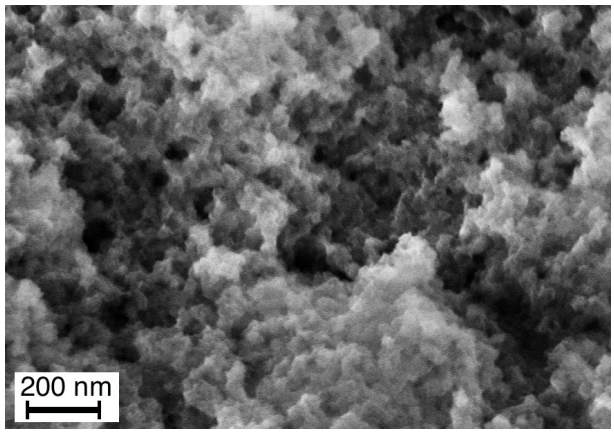

Figure 8. SEM image of MS_28d.

4. Discussion

The combined analysis of the results obtained by XRD, TG/DTA, SSNMR, and FTIR on MgO/SiO_2/water samples freeze-dried after 1, 7 and 28 days of hydration proves that the M-S-H binder phase is already present after the first 24 hours of hydration and keeps on forming during the monitored 28 days. In particular, the pH measurements, the X-ray diffraction and thermal data evidence that the reaction proceeds through the very fast hydration of MgO to form brucite, which is then consumed, until a small residual amount remains at 28 days. Concurrently, as highlighted by ^{29}Si SSNMR, silica is hydrated and consumed in 28 days of hydration. The increasing intensity of the characteristic broad peaks in XRD patterns indicates the progressive formation of M-S-H, which is definitely proved by ^{29}Si, ^{1}H and 2D ^{1}H-^{29}Si SSNMR experiments. The detailed analysis of ^{29}Si SSNMR spectra and, in particular, the obtainment of quantitative data allowed the different silicon species present in M-S-H to be identified and quantified.

The structural features of M-S-H deserve a particular discussion: indeed several hypotheses have been previously proposed in the literature, but an unambiguous description has not been achieved yet due to the strong amorphous character of the phase and the variety of techniques used for

its characterization. Moreover, although SSNMR is particularly powerful for the structural investigation of amorphous materials, its application to M-S-H has been quite limited so far; in particular, no quantitative data have been reported yet. In this work, the analysis of ^{29}Si SSNMR spectra of M-S-H revealed different silicon local environments: in particular a good spectral reproduction required at least two different signals for each Q^3 and Q^1 species and only one for Q^2 species. The most intense Q^3 signals, which arise from the fully condensed $\underline{Si}(OMg)(OSi)_3$ species, constituting the bulk of the material, can be exploited to recognize, inside the complex M-S-H phase, local silicon environments similar to those present in crystalline magnesium silicates, in the following indicated as "crystal-like" domains. It must be pointed out that, being the chemical shift a very local property, these similarities can be established independently of the presence of a long range order. Here the strongly amorphous character of M-S-H, as established from X-ray diffraction, implies a distribution of chemical structures, and consequently of ^{29}Si chemical shifts. Therefore the chemical shifts found for Q^{3A} and Q^{3B} species must be intended as those of the most representative "crystal-like" domains. In the attempt of describing the structure of M-S-H, it is common in the literature to take as models 2:1 or 1:1 magnesium phyllosilicates, constituted by T-O-T and T-O layers respectively, where T indicates a sheet of interconnected $(SiO_4)^{2-}$ tetrahedra and O stands for a sheet of Mg^{2+} cations octahedrally coordinated to hydroxyl groups and to the apical oxygen atoms of the T sheet(s). The ^{29}Si chemical shift of Q^{3A} (-92.9 ppm) coincides with that reported for the T-O phyllosilicate chrysotile,[34] a mineral of serpentine group, with formula $Mg_3Si_2O_5(OH)_4$ (see Figure 9A). On the other hand, the signal of Q^{3B} (-95.2 ppm) appears quite close to that reported for talc, a T-O-T phyllosilicate with formula $Mg_3Si_4O_{10}(OH)_2$ (see Figure 9B), whose Q^3 silicon nuclei resonate at about -97.7 ppm in the natural crystalline form, while a chemical shift of -95 ppm is reported for synthetic talc in the first stages of preparation.[33,45] The results obtained from the analysis of ^{1}H-^{29}Si CP-MAS spectra at variable contact time are interestingly in agreement with the proposed identification of Q^{3A} and Q^{3B} with silicon sites resembling those of chrysotile and talc. Indeed the shorter T_{SiH} observed for Q^{3A} with respect to Q^{3B} is in agreement with the larger number of ^{1}H nuclei (Mg-OH) contained in the formula of chrysotile. Further and stronger evidence of the coexistence of "talc-like" and "chrysotile-like" domains in M-S-H arises from XRD and SSNMR experiments carried out on heated samples. In fact the literature reports that, upon heating up to 900 °C, chrysotile converts mainly to forsterite (Mg_2SiO_4) and in part to enstatite ($MgSiO_3$),[34] while talc, especially if amorphous, transforms into enstatite.[33] XRD and SSNMR experiments on heated samples clearly show signals of both forsterite and clinoenstatite, a polymorph of enstatite already reported as a crystallization product of heated M-S-H gels.[27] These data show a prevalence of clinoenstatite, which can be explained also considering that further clinoenstatite could form at the expenses of forsterite.[33,34]

The almost complete absence of residual silica and brucite after 28 days of hydration (inferred from ^{29}Si SSNMR and XRD experiments, respectively) indicates that in the formed M-S-H phase Mg and Si are in an approximately 1:1 molar ratio, corresponding to the initial molar ratio between MgO and silica. The talc and chrysotile minimal formulas (respectively $Mg_3Si_4O_{10}(OH)_2$ and $Mg_3Si_2O_5(OH)_4$) suggest that in M-S-H the proportion between "talc-like" and "chrysotile-like" domains is approximately 1:1 by mole. This should be reflected in a 2:1 ratio between "talc-like" and "chrysotile-like" silicon species. From the 1:1 ratio between the quantitative areas of ^{29}Si signals of Q^{3A} and Q^{3B}, it can be derived that most of Q^2 silicon species in the MS_28d sample must be ascribed to "talc-like" domains.

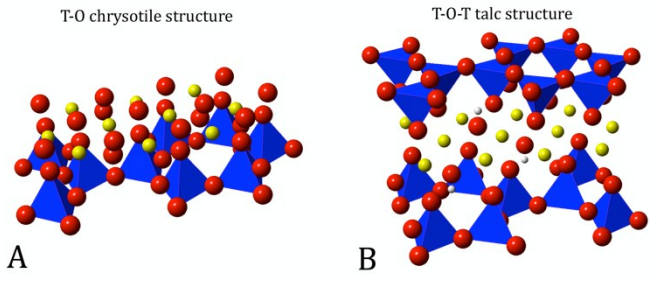

Figure 9. Scheme of (A) chrysotile (database code AMCSD: 0019917) and (B) talc (AMCSD: 0010839) structures. Blue tetrahedra represent Si species. Red, yellow and white spheres represent O, Mg and H atoms, respectively.

At last, it is worth to notice that the structure of M-S-H appears to be very much condensed since its early formation, with a very small presence of silanols. For the MS_28d sample, an average condensation degree of about 84% can be calculated as:

$$CD = 100(3Q^3 + 2Q^2 + Q^1) / 3(Q^3 + Q^2 + Q^1)$$

where the Q^i symbols are used for indicating the corresponding quantitative signal areas determined from ^{29}Si spectra. The composition of M-S-H as constituted by both "talc-like" and "chrysotile-like" domains is consistent with previous results.[21,30,46,47] In particular our data seem to well fit the description of "synthetic deweylite" given by Speakman and Majumdar as "a mixture of intimately interlayered badly crystallized talc and badly crystallized chrysotile".[48]
Two recent works proposed either talc[31] or lizardite[3] as best structural models of M-S-H, although the reported data are not incompatible with the coexistence of chrysotile and amorphous talc. Lizardite and chrysotile are polymorphs, differing in the arrangement of T-O layers: while lizardite shows flat sheets, chrysotile has cylindrical layers; this brings to a plate-like morphology for lizardite and to thin and flexible fibrils for chrysotile.[49] At the micrometric scale our M-S-H samples do not show typical chrysotile (or talc) morphology (Figure 8), as expected considering the assessed disordered structure constituted by mixed sub-nanometric sized "crysotile-like" and "talc-like" domains. However, it is known

that lizardite and chrysotile present some small structural differences at the sub-nanometric scale (weaker inter-layer hydrogen-bonds and slightly different thickness of the sheets in chrysotile)[50] that can be reflected by ^{29}Si chemical shift, reported to be -92.9 and -93.7 ppm for chrysotile and lizardite, respectively. Therefore the chemical shift of Q^{3A} sites suggests that the structural features of T-O domains in the M-S-H here investigated resemble much more chrysotile than lizardite.

5. Conclusions

Mixing highly reactive MgO and SiO_2 with water at room temperature, a M-S-H phase is formed already after the first 24 hours of hydration and its amount increases in the whole monitored period of 28 days. The reaction proceeds through the hydration of MgO to give $Mg(OH)_2$, which then reacts with silica. We used a multi-technique approach, including TG/DTA, XRD, FT-IR and SSNMR, to qualitatively and quantitatively follow the evolution of the hydration, as well as to obtain detailed structural information on M-S-H. The analysis of the data reveals that this reaction brings to the formation of an amorphous phase that is constituted by an intimate mixture of sub-nanometric sized domains with local structures resembling those of chrysotile and talc. The quantitative analysis of SSNMR data enabled us to conclude that the "talc-like" and "chrysotile-like" domains are approximately in a 1:1 molar ratio and that, on average, M-S-H has a high degree of condensation, corresponding to the presence of a small amount of silanols. Considering the strong amorphous character of M-S-H and the large variety of local structural motifs that can be formed, this work represents a significant step towards the detailed characterization of the M-S-H structure, which is of fundamental importance in view of the development of MgO-based eco-sustainable cements. The assessment of the M-S-H structure paves the way towards understanding and tailoring the macroscopic properties of the cement binder phase from the modification at the nanoscale.

Acknowledgements

This work was performed with the financial support of Ministero dell'Istruzione, Università e Ricerca scientifica MIUR (FIR2013 Project RBFR132WSM) and of Consorzio Interuniversitario per lo Sviluppo dei Sistemi a Grande Interfase, CSGI. Roberto Spiniello (ICCOM-CNR Pisa) is kindly acknowledged for its technical support.

References

1 T. Zhang, L. J. Vandeperre and C. R. Cheeseman, *J. Sustain. Cem.-Based Mater.*, 2012, **1**, 34.
2 K. -Y. Hwang, J. -Y. Seo, H. Q. H. Phan, J. -Y. Ahn and I. Hwang, *CLEAN - Soil Air Water*, 2014, **42**, 355.
3 S. A. Walling, H. Kinoshita, S. A. Bernal, N. C. Collier and J. L. Provis, *Dalton Trans.*, 2015, **44**, 8126.
4 L. J. Vandeperre, M. Liska, A. Al-Tabbaa and P. Claisse, in *Sustainable construction materials and technologies*, eds. T. R. Naik, E. Ganjian and Y. -M. Chun, Taylor & Francis/Balkema, Coventry, UK, 2007.
5 T. Zhang, C. R. Cheeseman and L. J. Vandeperre, *Cem. Concr. Res.*, 2011, **41**, 439.
6 F. Ridi, E. Fratini and P. Baglioni, *J. Coll. Interf. Sci.*, 2011, **357**, 255.
7 A. J. Hunt, E. H. K. Sin, R. Marriott and J. H. Clark, *ChemSusChem* 2010, **3**, 306.
8 E. A. Quadrelli, G. Centi, J. -L. Duplan and S. Perathoner, *ChemSusChem* **2011**, *4*, 1194.
9. M. Schneider, M. Romer, M. Tschudin and H. Bolio, *Cem. Concr. Res.*, 2011, **41**, 642.
10 E. M. Gartner and D. E. Macphee, *Cem. Concr. Res.*, 2011, **41**, 736.
11. R. J. Flatt, N. Roussel and C. R. Cheeseman, *J. Eur. Ceram. Soc.*, 2012, **32**, 2787.
12 F. Jin and A. Al-Tabbaa, *Cem. Concr. Compos.*, 2014, **52**, 27.
13 T. Zhang, L. J. Vandeperre and C. R. Cheeseman, *Cem. Concr. Res.*, 2014, **65**, 8.
14 Z. Li, T. Zhang, J. Hu, Y. Tang, Y. Niu, J. Wei and Q. Yu, *Constr. Build. Mater.*, 2014, **61**, 252.
15 J. Szczerba, R. Prorok, E. Śnieżek, D. Madej and K. Maślona, *Thermochim. Acta*, 2013, **567**, 57.
16 F. Jin and A. Al-Tabbaa, *Thermochim. Acta*, 2013, **566**, 162.
17 J. Wei, Q. Yu, W. Zhang and H. Zhang, *J. Wuhan Univ. Technol.-Mater. Sci. Ed.*, 2011, **26**, 745.
18 N. Vlasopoulos, Process for producing cement binder compositions containing magnesium. WO/2012/028471, March 8, 2012.
19 H. Dong, U. Cise, A. Al-Tabbaa and E. Yang, "Feasibility Study of Synthesizing MgO from Local Waste Brine Using Aqueous Ammonia" in *14th International Congress on the Chemistry of Cement*; Beijing, 2015; Vol. 1, pp 1.
20 H. M. Jennings and J. W. Bullard, *Cem. Concr. Res.*, 2011, **41**, 727.
21 D. R. M. Brew and F. P. Glasser, *Cem. Concr. Res.*, 2005, **35**, 85.
22 L. J. Vandeperre, M. Liska and A. Al-Tabbaa, *Cem. Concr. Compos.*, 2008, **30**, 706.
23 L. J. Vandeperre, M. Liska and A. Al-Tabbaa, *J. Mater. Civ. Eng.*, 2008, **20**, 375.
24 W. -S. Chiang, G. Ferraro, E. Fratini, F. Ridi, Y. -Q. Yeh, U. -S. Jeng, S. -H. Chen and P. Baglioni, *J. Mater. Chem. A*, 2014, **2**, 12991.
25 M. Geppi, S. Borsacchi, G. Mollica and C. A. Veracini, *Appl. Spectrosc. Rev.*, 2008, **44**, 1.
26. A. Rawal, B. J. Smith, G. L. Athens, C. L. Edwards, L. Roberts, V. Gupta and B. F. Chmelka, *J. Am. Chem. Soc.* 2010, **132**, 7321.
27 J. S. Hartman and R. L. Millard, *Phys. Chem. Miner.*, 1990, **17**, 1.
28 J. -B. d' Espinose de la Caillerie, M. Kermarec and O. Clause, *J. Phys. Chem.*, 1995, **99**, 17273.
29 J. Temuujin, K. Okada and K. J. D. MacKenzie, *J. Am. Ceram. Soc.*, 1998, **81**, 754.
30 J. Temuujin, K. Okada and K. J. D. MacKenzie, *J. Solid State Chem.*, 1998, **138**, 169.
31 C. Roosz, S. Grangeon, P. Blanc, V. Montouillout, B. Lothenbach, P. Henocq, E. Giffaut, P. Vieillard and S. Gaboreau, *Cem. Concr. Res.*, 2015, **73**, 228.
32 E. M. Van der Merwe, C. Strydom and A. Botha, *J. Therm. Anal. Calorim.*, 2004, **77**, 49
33 K. J. D. MacKenzie and R. H. Meinhold, *Thermochim. Acta*, 1994, **244**, 195
34 K. J. D. MacKenzie and R. H. Meinhold, *Am. Mineral.*, 1994, **79**, 43.
35 O. Mendoza, G. Sierra and J. I. Tobón, *Constr. Build. Mater.*, 2014, **54**, 550.

36 J. Dweck, P. F. Ferreira da Silva, P. M. Büchler and F. K. Cartledge, *J. Therm. Anal. Calorim.*, 2002, **69**, 179.
37 F. Guirado, S. Galí and J. S. Chinchón, *Cem. Concr. Res.*, 1998, **28**, 381.
38 X. Xue and M. Kanzaki, *J. Phys. Chem. B*, 2007, **111**, 13156.
39 C. C. Liu and G. E. Maciel, *J. Am. Chem. Soc.*, 1996, **118**, 5103.
40 C. E. Bronnimann, R. C. Zeigler and G. E. Maciel, *J. Am. Chem. Soc.*, 1988, **110**, 2023.
41 R. Freeman, H.D.W. Hill *J. Chem. Phys.*, 1971, **54**, 3367.
42 B. Pfleiderer, K. Albert, E. Bayer, L. Van de Ven, J. De Haan and C. Cramers, *J. Phys. Chem.*, 1990, **94**, 4189.
43 V. I. Bakhmutov, *Chem. Rev.*, 2011, **111**, 530.
44. "http://rruff.info/Brucite/R050455"
45 A. Dumas, F. Martin, C. Le Roux, P. Micoud, S. Petit, E. Ferrage, J. Brendlé, O. Grauby and M. Greenhill-Hooper, *Phys. Chem. Miner.*, 2013, **40**, 361.
46 G. L. Kalousek and D. Mui, *J. Am. Ceram. Soc.*, 1954, **37**, 38.
47 J. C.-S. Yang, *J. Am. Ceram. Soc.*, 1960, **43**, 542.
48 K. Speakman and A. J. Majumdar, *Mineral Mag.*, 1971, **38**, 225.
49 C. Rinaudo, D. Gastaldi and E. Belluso, *Can. Mineral.*, 2003, **41**, 883.
50 F. J. Wicks and E. J. W. Whittaker, *Can. Mineral.*, 1975, **13**, 227.

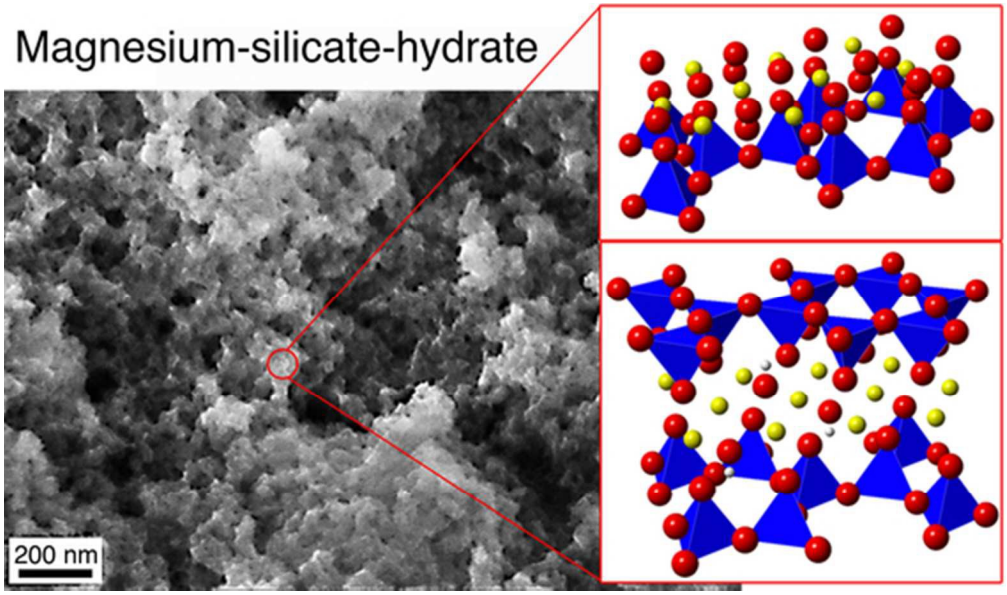

48x28mm (300 x 300 DPI)